32nd AIAA Fluid Dynamics Conference and Exhibit
24-26 June 2002, St. Louis, Missouri

AIAA 2002-2961

# AIAA 2002–2961

## High Reynolds-Number Assessment of a Multifractal Subgrid-Scale Model

Gregory C. Burton, Werner J.A. Dahm, David R. Dowling
and Kenneth G. Powell

*Laboratory for Turbulence and Combustion*
*Department of Aerospace Engineering*
*The University of Michigan, Ann Arbor, MI 48109-2140*

*W. M. Keck Foundation Laboratory for Computational Fluid Dynamics*
*Department of Aerospace Engineering*
*The University of Michigan, Ann Arbor, MI 48109-2140*

**32nd AIAA Fluid Dynamics Conference and Exhibit**
**June 24–26, 2002/St. Louis, MO**

# High Reynolds-Number Assessment of a Multifractal Subgrid-Scale Model

Gregory C. Burton,* Werner J.A. Dahm,† David R. Dowling‡
and Kenneth G. Powell§

*Laboratory for Turbulence and Combustion*
*Department of Aerospace Engineering*
*The University of Michigan, Ann Arbor, MI 48109-2140*

*W. M. Keck Foundation Laboratory for Computational Fluid Dynamics*
*Department of Aerospace Engineering*
*The University of Michigan, Ann Arbor, MI 48109-2140*

**We report further results from our *a priori* assessment of a multifractal subgrid-scale model for large-eddy simulation. In this paper, we compare the model's ability to recover components of the subgrid-stress tensor $\tau_{ij}^*$ and the subgrid energy-production $\mathcal{P}^*$ field in low and high Reynolds-number turbulence, ($Re_\lambda \sim 160$ and $Re_\lambda \sim 2550$). We find that in comparisons with DNS data, the model recovers $\tau_{ij}^*$ with correlations of $\rho \sim 0.855$ and $\rho \sim 0.635$ in the lower and higher-Re cases, respectively. We also report correlations between DNS and model values for the SGS energy-production field $\mathcal{P}^*$ of $\rho \sim 0.860$ in the lower Reynolds-number context and $\rho \sim 0.804$, in the more turbulent flow. We further examine the model's ability to recover components of the averaged subgrid-velocity field $\overline{\boldsymbol{u}^{sgs}}$, which shows correlations of $\rho \sim 0.915$. We also analyze the individual terms within the decomposition of $\tau_{ij}^*$ itself. These tests in sum indicate that the present multifractal model recovers significant structural characteristics of the subgrid field. The comparisons also suggest possible higher-order refinements to the model. Finally, we set forth in some detail a multifractal model for the Reynolds stresses in the Reynolds-Averaged Navier-Stokes equations.**

## 1. Introduction.

In our previous paper Burton *et al* (2002), we presented a fundamentally new approach to the modeling of the subgrid-scale stresses for the large-eddy simulation (LES) of turbulent flows based on the multifractal structure of the subgrid-vorticity field in high Reynolds-number turbulence. That paper set forth in some detail the physical bases for representing the spatial distribution of subgrid vorticity with a multifractal model and the derivation of an expression for the subgrid velocity field based on multifractal concepts. We also reported on an initial series of *a priori* tests comparing DNS and model values. In the present paper, we briefly summarize the derivation of the model and the results of those initial *a priori* tests. We then describe in some detail further *a priori* tests, in which the model and DNS values are compared in lower and higher Reynolds-number contexts. In the final section, we set forth the derivation of a multifractal model for the Reynolds stresses in the Reynolds-averaged Navier-Stokes equation.

## 2. Review of Multifractal Model.

The present multifractal model is based on a representation of the spatial distribution of vorticity magnitudes and orientations within the subgrid field of an individual LES grid-cell. These distributions are then inserted into the Biot-Savart operator to derive the subgrid-velocity field $\boldsymbol{u}^{sgs}$ that permits direct calculation of the individual terms in the SGS stress tensor

$$\tau_{ij} = \overline{\overline{u_i}\,\overline{u_j}} + \overline{\overline{u_i}\,u_j^{sgs}} + \overline{u_i^{sgs}\,\overline{u_j}} + \overline{u_i^{sgs}\,u_j^{sgs}} \qquad \overline{u_i}\,\overline{u_j}. \tag{1}$$

We believe this to be the first LES approach involving explicit calculation of each term within the decomposition of the SGS stress tensor. The stress tensor $\tau_{ij}$ can be further separated into resolved $\tau_{ij}^R$ and subgrid $\tau_{ij}^*$ components, where

$$\tau_{ij} \equiv \tau_{ij}^R + \tau_{ij}^*. \tag{2}$$

*FXB Fellow, Member AIAA, Corresponding Author.
†Professor, Associate Fellow AIAA.
‡Associate Professor.
§Professor, Member AIAA.

The resolved component $\tau_{ij}^R$, defined as

$$\tau_{ij}^R \equiv \overline{\overline{u_i}\,\overline{u_j}} \qquad \overline{u_i}\,\overline{u_j}, \tag{3}$$

concerns the resolved scales of the flow exclusively, and is obtained directly from the LES flow solver. As such, it is completely unrelated to the subgrid model proposed here. By contrast, the subgrid component $\tau_{ij}^*$, defined as

$$\tau_{ij}^* \equiv \overline{\overline{u_i} u_j^{sgs}} + \overline{u_i^{sgs} \overline{u_j}} + \overline{u_i^{sgs} u_j^{sgs}}, \tag{4}$$

contains all of the contributions of the modeled subgrid field to the value of the full stress-tensor in (1). By isolating all of the turbulence modeling in $\tau_{ij}^*$ and removing purely resolved quantities to $\tau_{ij}^R$, this decomposition permits us to focus exclusively on the adequacy of our multifractal model for the subgrid scales. Therefore the following analysis will be concerned solely with $\tau_{ij}^*$ and the related subgrid energy-production field $\mathcal{P}^*$, defined as

$$\mathcal{P}^* \equiv \quad \tau_{ij}^*\, \overline{S}_{ij}. \tag{5}$$

*A. Summary of Model Derivation.*

The present multifractal model draws on numerous computational, theoretical and experimental studies indicating that certain gradient quantities in turbulent flows, such as enstrophy $\frac{1}{2}\boldsymbol{\omega}\cdot\boldsymbol{\omega}$, display multifractal scale-similar structure within inertial-range scales in high-Reynolds number turbulence. As discussed more fully in Burton *et al* (2002), this multifractal structure permits the spatial distribution of vorticity magnitudes within the subgrid field to be represented by a multiplicative cascade. The total amount of enstrophy distributed within the subgrid field $Q_{sgs}$ is determined from a Kolmogorov spectral analysis, derived from integrating the enstrophy spectrum $\mathcal{Q}(k)$ from the smallest-resolved scale $\Delta$ to the viscous scale $\lambda_\nu$, where

$$Q_{sgs} = \frac{3}{4}\, Q_\Delta \left[ \left( \frac{k_\nu}{k_\Delta} \right)^{\frac{4}{3}} \quad 1 \right]. \tag{6}$$

Thus, the spatial distribution of vorticity magnitude can then be represented as

$$|\omega^{sgs}(\mathbf{x},t)| = \left[ Q_{sgs} \prod_{i=1}^{\Delta/\lambda_\nu} \left(M_\varepsilon(\mathbf{x},t)\right)_i \right]^{\frac{1}{2}}. \tag{7}$$

Based on analysis of high Reynolds-number DNS data, the distribution of vorticity orientations within a single LES grid cell can be represented by an additive cascade describing the isotropic decorrelation of vorticity orientations through the subgrid field from the orientations at scale $\Delta$. This decorrelation process can be represented as

$$\hat{\mathbf{e}}_i^{sgs}(\mathbf{x},t) = C_\mathcal{M} \left[ \hat{\mathbf{e}}_i^\Delta(\mathbf{x},t) \quad + \quad \delta_i^{sgs}(\mathbf{x},t) \right], \tag{8}$$

where $\hat{\mathbf{e}}^\Delta$ represents the vorticity orientation at scale $\Delta$, and $\delta_i^{sgs}$ represents the summation of decorrelation angles through the subgrid scales. The averaged normalization constant $C_\mathcal{M}$ is defined as

$$C_\mathcal{M} \equiv \frac{1}{\sqrt{1 + 2\sqrt{3\mathcal{M}}\,\sigma + 3\mathcal{M}\sigma^2}}, \tag{9}$$

where $\mathcal{M}$ represents the number of scales within the subgrid field and $\sigma$ is the r.m.s. value of the probability distribution, identified from analysis of DNS data, from which the orientation cascade is constructed. This factor is necessary to ensure that on average the resultant orientation vector $\hat{\mathbf{e}}^{sgs}$ in (8) is of unit length.

The multifractal magnitude cascade and the additive orientation cascade together provide a rigorous representation for the spatial distribution of vorticity within the subgrid scales. Using the Biot-Savart operator, we now can derive an exact analytical expression for the subgrid velocity components $u_i^{sgs}$ appearing in the SGS stress tensor, as

$$\begin{aligned} u_i^{sgs} \quad = \quad & \underbrace{\frac{1}{4\pi} \int_{\mathbf{x}'} \left[ (C_\mathcal{M}\, |\boldsymbol{\omega}^{sgs}|\, \hat{\mathbf{e}}^\Delta) \times \mathbf{K} \right] \cdot \hat{e}_i \; d^3\mathbf{x}'}_{\mathcal{S}^\Delta:\, Resolved \quad Orientation} \\ & + \underbrace{\frac{1}{4\pi} \int_{\mathbf{x}'} \left[ (C_\mathcal{M}\, |\boldsymbol{\omega}^{sgs}|\, \delta^{sgs}) \times \mathbf{K} \right] \cdot \hat{e}_i \; d^3\mathbf{x}'}_{\mathcal{S}^\phi:\, Subgrid\ Decorrelation}, \end{aligned} \tag{10}$$

where $|\,\boldsymbol{\omega}^{sgs}|$ is substituted for the magnitude expression in (7). The continuous integrals $\mathcal{S}^\Delta$ and $\mathcal{S}^\phi$ in (10) can be approximated by a discrete summation over all subgrid cells of volume $\lambda_\nu^3$. Since both summations involve stochastic quantities, they can be analyzed using central-limit concepts, and in the high Reynolds-number limit, the components of the subgrid velocity field $u_i^{sgs}$ can be represented by the simple functional form,

$$u_i^{sgs}(\mathbf{x},t) \;\approx \mathcal{C}(\mathbf{x},t)\; \hat{\mathbf{e}}_i^{\mathbf{u}^\Delta}(\mathbf{x},t), \tag{11}$$

where

$$\mathcal{C}(\mathbf{x},t) \;\equiv\; C_\mathcal{M}\, |\mathbf{u}^\Delta(\mathbf{x},t)| \frac{|\boldsymbol{\omega}^{sgs}(\mathbf{x},t)|}{|\boldsymbol{\omega}^\Delta(\mathbf{x},t)|}. \tag{12}$$

The subgrid velocity field $\boldsymbol{u}^{sgs}$ is now expressed solely in terms of quantities available from the resolved scales of the flow. The SGS stress tensor $\tau_{ij}^*$ therefore can be represented as

$$\tau_{ij}^* \;=\; \overline{\overline{u_i}\, \mathcal{C}\, \hat{\mathbf{e}}_j^{\mathbf{u}^\Delta}} \;+\; \overline{\mathcal{C}\, \hat{\mathbf{e}}_i^{\mathbf{u}^\Delta}\, \overline{u_j}} \;+\; \overline{\mathcal{C}\, \hat{\mathbf{e}}_i^{\mathbf{u}^\Delta}\, \mathcal{C}\, \hat{\mathbf{e}}_j^{\mathbf{u}^\Delta}}, \tag{13}$$

which is the final form of the present multifractal subgrid-scale model. Note that the remaining portion of the SGS stress tensor $\tau_{ij}^R$ defined in (3) contains no subgrid quantities and is a function only of the resolved-velocity field, which is available directly from the LES flow solver. It is thus unrelated to the evaluation of the model examined here. For a complete discussion of the foregoing derivation, see Burton *et al* (2002).

### *B. Summary of Prior Validation Tests.*

The prior paper also reported the results of an initial series of *a priori* tests comparing model and DNS values, in order to assess the validity of the multifractal model and the assumptions underlying its derivation. The comparisons were made using high-resolution ($N = 512^3$) DNS data with an estimated Taylor-scale Reynolds number of $Re_\lambda \sim 168$. This data was then spatially filtered at $16dx$ to create LES resolved and subgrid-velocity fields each containing $32^3$ data points. Multifractal analysis of the DNS data set forth in our previous paper indicates that the resulting subgrid velocity-fields contain four inertial range scales as well as additional viscous scales. Using the relation discussed in Buch & Dahm (1998),

$$\frac{\lambda_\nu}{\Delta} = 11.2\ Re_\Delta{}^{\frac{3}{4}}, \tag{14}$$

we estimate the effective cell-Reynolds number of the LES subgrid fields examined in these prior tests to be $Re_\lambda \sim 160$.

In these initial *a priori* tests, we examined the model's ability to recover three relevant characteristics of the LES flow: *(i)* the filtered subgrid-velocity components $\overline{u_i^{sgs}}$, *(ii)* the components of the subgrid-stress tensor $\tau_{ij}^*$, and *(iii)* the SGS-energy production field $\mathcal{P}^*$. The recovery of the filtered components of the subgrid-velocity field $\overline{u_i^{sgs}}$ was a direct means of assessing the accuracy of the model, which explicitly represents the subgrid velocity field. Here global correlations between the DNS and model values were calculated to be $\rho \sim 0.91$. The model exhibited good magnitude as well as spatial agreement, indicating its ability to recover significant structural characteristics of the field. We also reported comparisons of DNS and model values for the SGS stress tensor $\tau_{ij}^*$ and the subgrid energy-production field $\mathcal{P}^*$. For both fields, we found high correlations $\rho \sim 0.85$, as well as good magnitude agreement, indicating that the model recovers much of the true spatial structure of the subgrid-stress tensor and subgrid energy-production fields. For a complete discussion of these prior tests, see Burton *et al* (2002).

## 3. A Priori Tests at Higher Reynolds-Number.

### *A. Preparation of High Re DNS Fields.*

Since our previous paper, we have conducted additional *a priori* comparisons of our multifractal model against pre-existing DNS data. Because the present model was derived by way of a high Reynolds-number limit analysis, we sought to make these additional tests in a higher Reynolds-number context, where the DNS velocity fields contain a larger number of subgrid scales. To derive such fields, we first filtered the same DNS dataset used in the earlier studies with a spherically-symmetric spectrally-sharp filter to remove the viscous scales of the flow. The resulting fields were then filtered in the spatial domain using a three-dimensional top-hat filter of width $\Delta = 128dx$ to create the resolved and subgrid LES fields. This procedure produced LES resolved-velocity fields containing four scales and LES subgrid fields containing 32 scales within each of $4^3$ LES grid cells. As a result, the effective cell-Reynolds number for these fields was estimated to be $Re_\lambda \sim 2550$, significantly higher than in the previous *a priori* studies. Since four separate time realizations were available from the DNS simulations, this permitted DNS vs. model comparisons at a total of 256 LES data points, an adequate number to make a statistically credible assessment of the model's performance in the higher Reynolds-number context.

### *B. Numerical Implementation.*

As set forth above, the model expresses the subgrid velocities appearing in the decomposition of $\tau_{ij}^*$ as a functions of quantities at the smallest resolved scale $\Delta$, *i.e.*,

$$u_i^{sgs} \equiv \mathcal{F}\left(|\mathbf{u}^\Delta|, |\boldsymbol{\omega}^\Delta|, |\boldsymbol{\omega}^{sgs}|, \hat{\mathbf{e}}_i^{\mathbf{u}^\Delta}\right) \equiv \mathcal{F}\left(\mathcal{C}, \hat{\mathbf{e}}_i^{\mathbf{u}^\Delta}\right). \tag{15}$$

Each of these quantities represents a continuous field which is sampled on the LES grid. These fields, in turn, appear under a filtering operator in the expression for the SGS stress tensor in (4), which here is taken to represent a three-dimensional spatial average over a single LES grid-cell of size $\Delta^3$. Thus, calculation of each term within the decomposition of $\tau_{ij}^*$ requires selecting continuous representations of all fields, which are combined, integrated and then averaged in each LES grid cell. Thus a single term in $\tau_{ij}^*$ — for example, $\overline{u_i^{sgs}\,\overline{u_j}}$ — can be calculated as

$$\overline{u_i^{sgs}\,\overline{u_j}} = \overline{\mathcal{C}\,\hat{\mathbf{e}}_i^{\mathbf{u}^\Delta}\,\overline{u_j}} = \frac{1}{\Delta^3}\int \left(\mathcal{C}\,\hat{\mathbf{e}}_i^{\mathbf{u}^\Delta}\overline{u_j}\right) d^3\mathbf{x}'. \tag{16}$$

In the present study, we employ quadratic representations of all resolved field quantities. The gradients

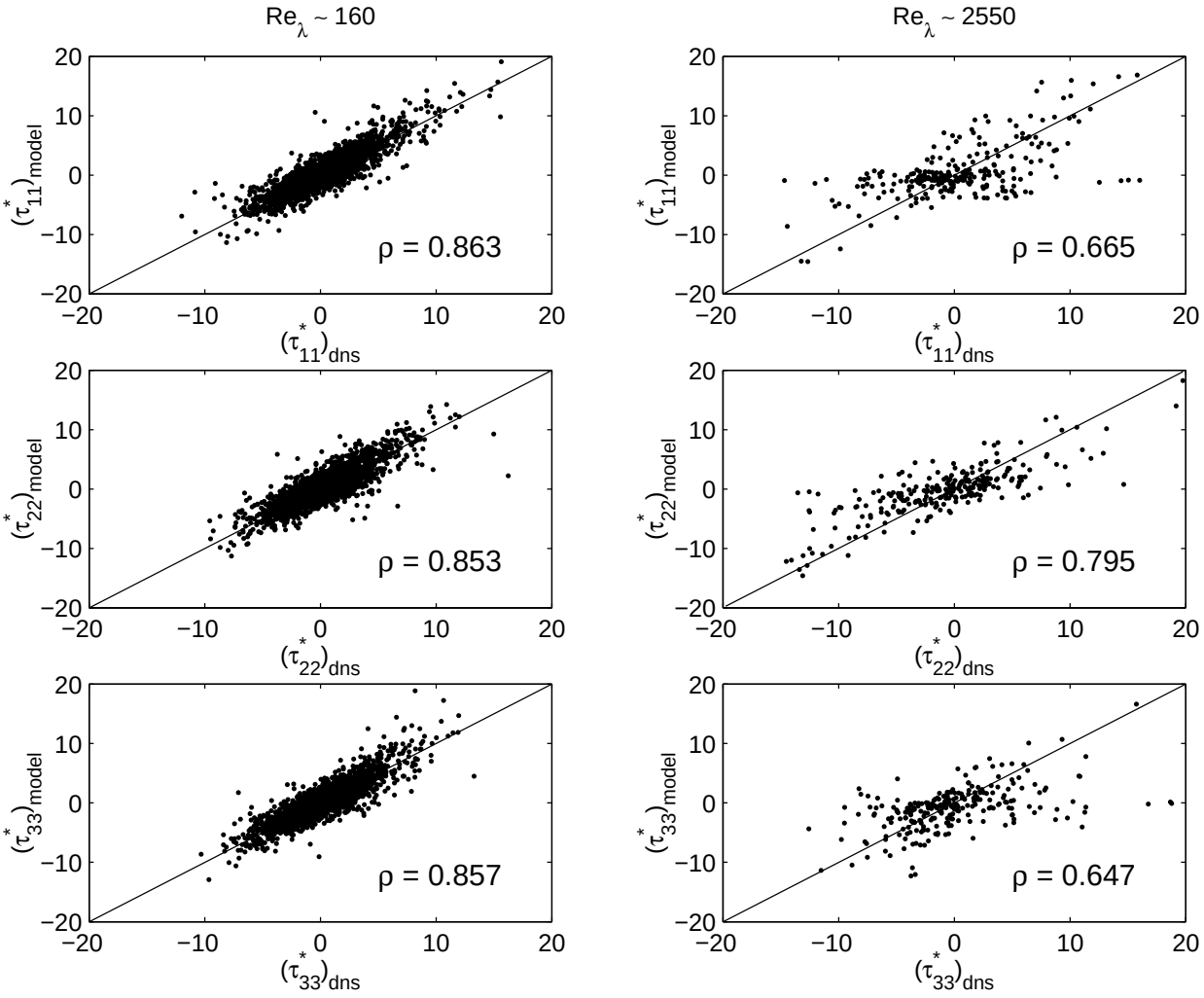


**Fig. 1 Normal components of the subgrid stress tensor $\tau^*_{ij}$ defined in (4). The illustrated scatterplots compare DNS vs. model values at lower and higher Reynolds numbers ($Re_\lambda \sim 160$ and $Re_\lambda \sim 2550$, *left and right columns, respectively*). Correlations were found to be greater in the lower-Re context, $\rho \sim 0.858$, than in the higher-Re flow, where $\rho \sim 0.703$. Mean normalized $L^2$ error was found to be 0.826 in the lower Reynolds-number case as compared with 1.001 in the higher Reynolds-number case.**

in these representations are determined by an unweighted least-squares approximation based on the twenty-six nearest neighbors of an individual LES grid-cell.

### *C. The SGS Stress Tensor, $\tau^*_{ij}$.*

We first compared the ability of the multifractal model to recover the orientations and magnitudes of the component fields of the SGS stress tensor $\tau^*_{ij}$ in lower and higher Reynolds-number contexts. Our assessment consisted of calculating correlation coefficients to quantify phase agreement and $L^2$ errors to assess magnitude agreement of the modeled quantities. The error statistics were calculated after each field was normalized by the mean absolute value of the relevant DNS quantity. In addition, we produced scatterplots of each component, comparing DNS and model values, in order to assess visually the performance of the model.

Figure 1 sets forth scatterplots for the normal components of $\tau^*_{ij}$ in the lower and higher Reynolds-number contexts (*left and right columns, respectively*). Mean correlations between the DNS and model values in the lower Reynolds-number flow were calculated to be $\rho \sim 0.858$, and were somewhat smaller in the higher-Re case $\rho \sim 0.703$. Examination of the mean normalized $L^2$ error indicated that the model produced slightly smaller global error in the lower Reynolds-number case 0.826, than in the higher-Re case, which produced an error of 1.001.

The model recovered the shear-component fields of $\tau^*_{ij}$ in similar fashion. As illustrated in Figure 2, mean correlations were determined to be $\rho \sim 0.856$ for the lower Reynolds-number data and $\rho \sim 0.604$ for the higher-Re data, slightly lower than the corresponding statistics for the normal tensor-component fields. For the shear-component fields, the model produced a mean normalized $L^2$ error of 0.849 in

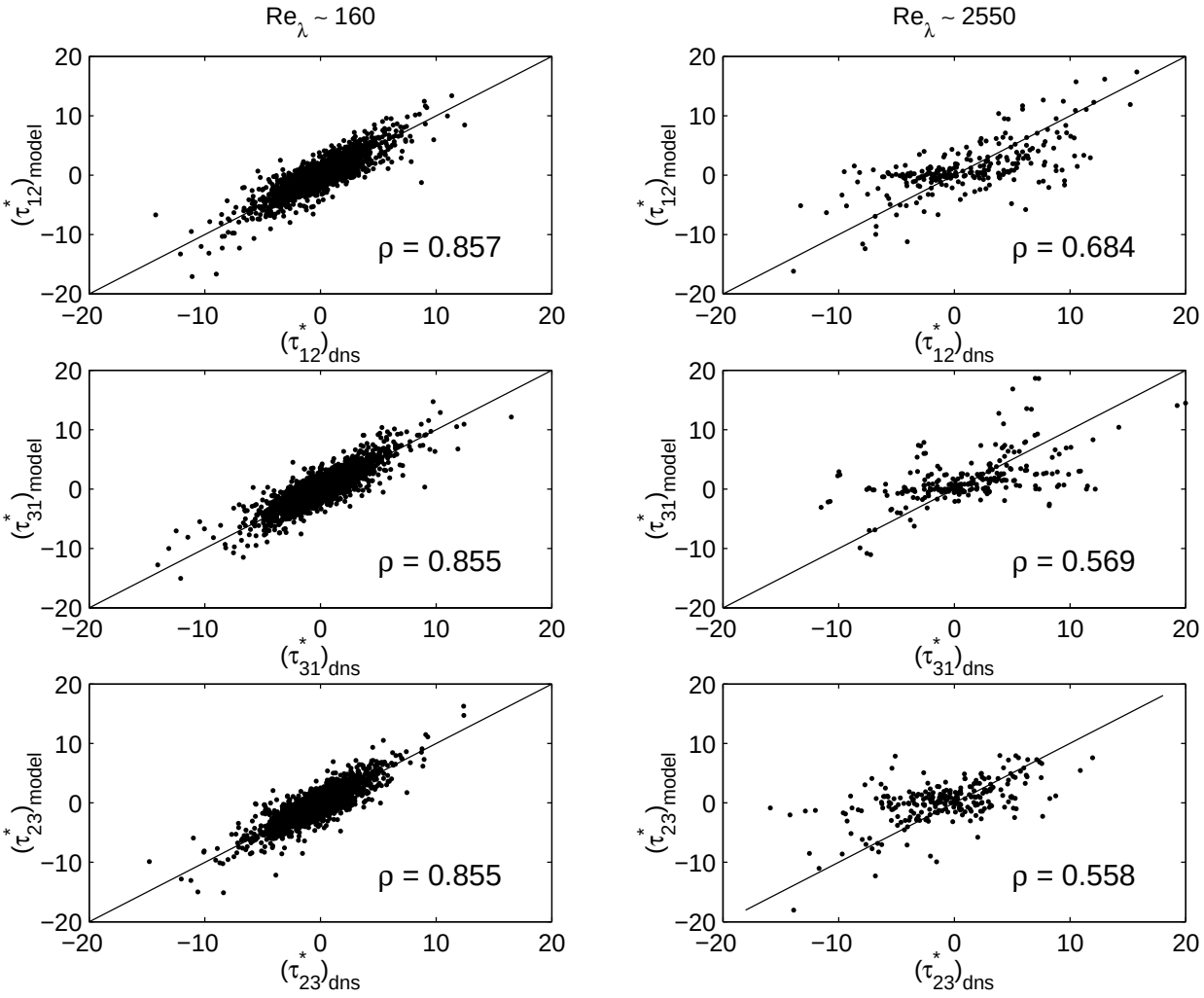


**Fig. 2 Shear components of the subgrid-stress tensor $\tau^*_{ij}$ defined in (4). The scatterplots compare DNS vs. model values in lower and higher Reynolds-number flows (*left and right columns, respectively*). As with the normal-tensor components, the lower Reynolds-number context exhibits higher correlations, $\rho \sim 0.856$, than the higher Reynolds-number context where $\rho \sim 0.604$. In the less turbulent flow, the model produces a slightly smaller mean normalized $L^2$ error of $0.849$, when compared with the higher Reynolds-number flow, with an $L^2$ error of $1.052$.**

the lower-Re case and 1.052 in the higher-Re case. This suggests that, as with the normal components, the model is slightly better able to recover magnitude characteristics of the shear tensor-component fields in the lower Reynolds-number context.

### *D. SGS Energy Production Field, $\mathcal{P}^*$.*

We next examined the model's ability to recover the orientations and magnitudes of the SGS energy production field, $\mathcal{P}^*$. This is an important test for a subgrid-scale model, since proper calculation of the energy transfer between the resolved and subgrid fields is essential in any effective LES calculation. As set forth in Figure 3, the model produces high correlations of $\rho \sim 0.860$ and $\rho \sim 0.804$, in the lower and higher Reynolds-number contexts, respectively, in comparisons with the DNS data. The model calculates the magnitude of $\mathcal{P}^*$ with slightly greater accuracy in the lower-Re context. There, the normalized $L^2$ error was determined to be 0.937, as compared with 0.952 in the higher-Reynolds number case. These analyses indicate that the present multifractal model is able to recover important characteristics of the subgrid-stress tensor $\tau^*_{ij}$ and SGS energy production $\mathcal{P}^*$ fields, in both lower and higher Reynolds-number flows.

### *E. Analyses of $\boldsymbol{u}^{sgs}$ and Individual Terms of $\tau^*_{ij}$.*

We next explored the model's ability to recover the components of the filtered subgrid-velocity field $\overline{u_i^{sgs}}$ as well as the three individual terms within the decomposition of $\tau^*_{ij}$ in (4). These tests provide additional insight into the behavior of the model in lower and higher Reynolds-number contexts.

As discussed previously, the present model draws upon multifractal concepts to represent the subgrid-

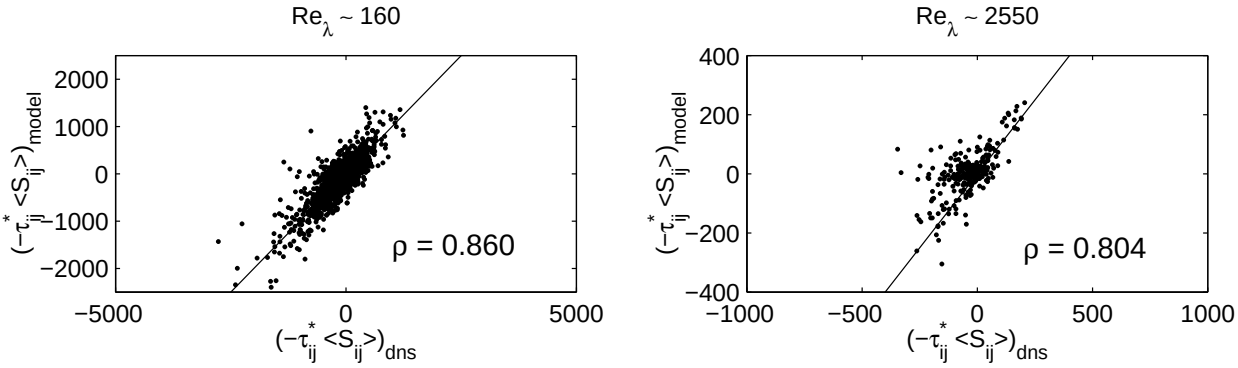


**Fig. 3 The SGS energy-production field $\mathcal{P}^*$ defined in (5), comparing DNS vs. model data. The model produces slightly higher correlations in the lower Reynolds-number flow, $\rho \sim 0.860$, than the higher Reynolds-number flow, where $\rho \sim 0.804$. The normalized $L^2$ error was also slightly smaller in the lower Reynolds-number context, 0.937, when compared with the more turbulent flow, where the $L^2$ error was 0.952.**

velocity field. A basic test of the model, therefore, is its ability to recover the components of the filtered subgrid-velocity field $\overline{u_i^{sgs}}$. As illustrated in Figure 4, the model captures most of the orientation and magnitude characteristics of the DNS fields, producing global correlations of approximately $\rho \sim 0.91$ in the lower-Re case and $\rho \sim 0.92$ in the higher-Re case. This indicates excellent phase agreement between model and DNS values. The model produces a mean normalized $L^2$ error of 0.586 in the lower-Re case. This improves somewhat in the higher-Re context, with an $L^2$ error of 0.486, reflecting a 18% reduction over the less turbulent flow. These results demonstrate that the model recovers significant magnitude and orientation structure of the filtered subgrid-velocity field $\overline{u_i^{sgs}}$.

We next evaluated the ability of the multifractal model to recover the two cross terms, $\overline{\overline{u_i}\, u_j^{sgs}}$ and $\overline{u_i^{sgs}\,\overline{u_j}}$, within the decomposition of the subgrid stress tensor $\tau^*_{ij}$ in (4). These terms represent the averaged interaction of the resolved and subgrid velocity fields within an individual LES grid cell. Figure 5 (*top and middle*) illustrates that substantial characteristics of these fields are captured by the multifractal model in both the lower and higher Reynolds-number contexts. Global correlations were determined to be $\rho \sim 0.88$ for both terms in the lower-Re case and $\rho \sim 0.73$ in the higher-Re case. The model produced a mean normalized $L^2$ error 0.797 in the lower Reynolds-number case, as compared with an error of 0.963 seen in the higher Reynolds-number context. This is consistent with other results in which the lower Reynolds-number cases produced the slightly smaller error.

Finally, we evaluated the model's ability to recover the subgrid-subgrid term $\overline{u_i^{sgs}\, u_j^{sgs}}$ in the decomposition of $\tau^*_{ij}$ in (4). This term represents the averaged value of all subgrid-subgrid interactions within a given LES grid cell. Here we note that the model produces lower correlations and higher magnitude errors than for any other quantity examined. As illustrated in Figure 5 (*bottom*), the correlations for both the lower and higher Reynolds-number cases, were determined to be $\rho \sim 0.361$ and $\rho \sim 0.298$, respectively. Similarly, the model produces normalized $L^2$ errors of 1.460 and 1.182 in the lower and higher Reynolds-number contexts, respectively. These results suggest that in its present form the model may not fully capture certain characteristics of subgrid-subgrid interactions, and that it is these interactions that are mostly responsible for the slightly diminished results reported in the higher Reynolds-number context. We are presently refining our multifractal model to account more faithfully for these subgrid-subgrid interactions in light of these results.

## 4. A Multifractal RANS Closure Model.

The present multifractal model can be readily extended to model the Reynolds stresses in the Reynolds-averaged Navier-Stokes (RANS) equations,

$$\frac{\partial\, \widetilde{u}_i}{\partial t} + \widetilde{u}_j \frac{\partial\, \widetilde{u}_i}{\partial x_j} \quad \nu \frac{\partial^2\, \widetilde{u}_i}{\partial x_j \partial x_j} = \quad \frac{\partial\, \widetilde{p}}{\partial x_i} + \quad \frac{\partial}{\partial x_j}\, \widetilde{u_i' u_j'}. \tag{17}$$

Note that the averaging operator denoted by $(\,\widetilde{\cdot}\,)$ in (17) represents a time average at a given spatial location. By contrast, the present multifractal model provides a spatial representation of the subgrid-vorticity field in a single LES grid cell, from which a representation of the subgrid velocity field is derived. Using Taylor's hypothesis, which relates the temporal and spatial gradients, through the mean flow $\overline{U}$ as

$$\frac{\partial}{\partial t} \sim \quad \overline{U}\, \frac{\partial}{\partial x}\,, \tag{18}$$

it can be shown that the spatial and temporal

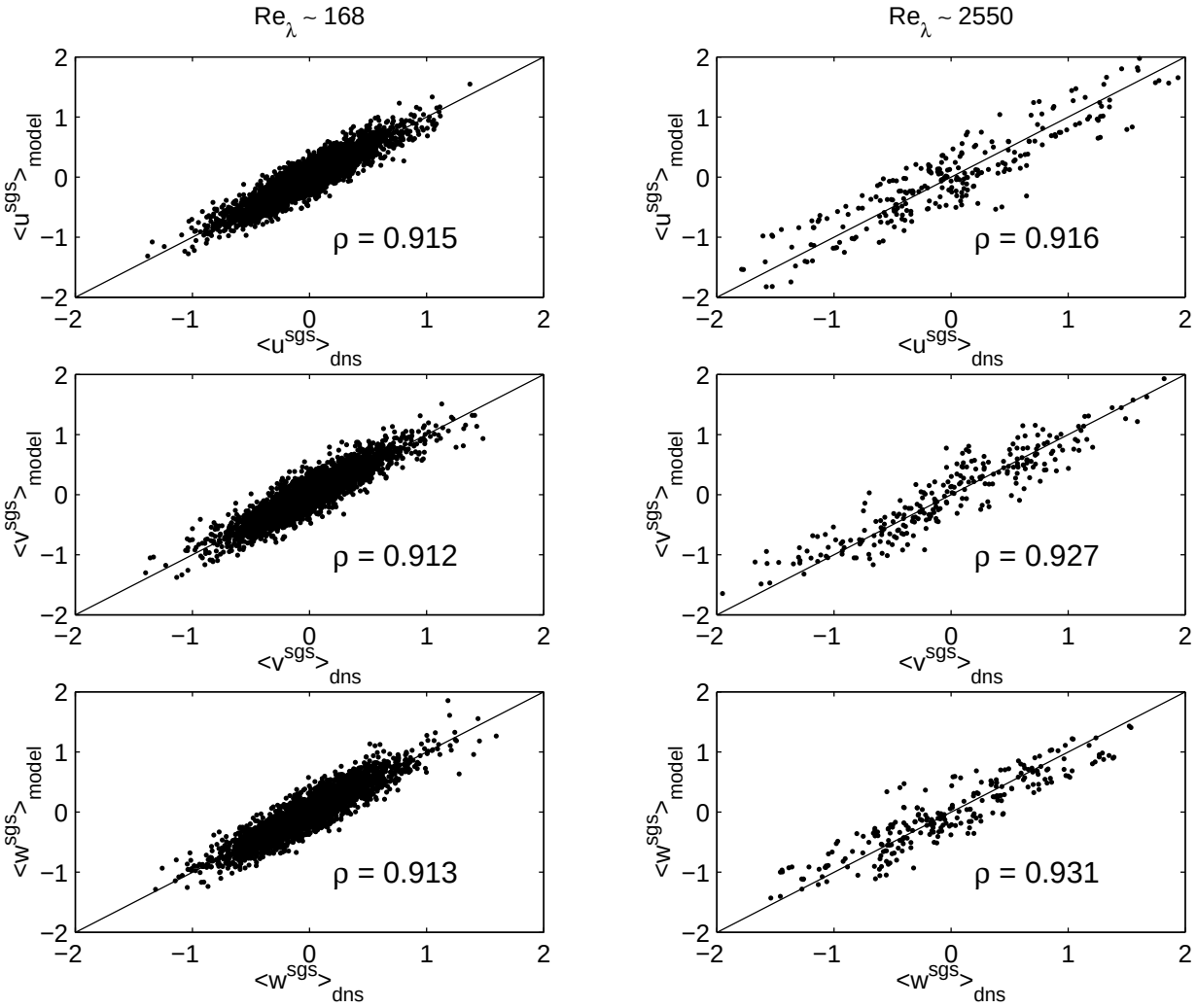


**Fig. 4 Filtered subgrid-velocity components $\overline{u_i^{sgs}}$ at low and high Reynolds number, comparing DNS vs. model values. This is a fundamental test of the multifractal model, which explicitly represents the components of the SGS velocity field. In both the low and high Reynolds-number cases, the multifractal model produces correlations globally averaging $\rho \sim 0.92$. The model also produced mean normalized $L^2$ errors of $0.586$ and $0.486$ in the lower-Re and higher-Re contexts, respectively. These results indicate excellent agreement between the model and DNS values.**

domains are equivalent for purposes of deriving a spatially-based model for the Reynolds stresses, *i.e.* that

$$\widetilde{u_i^{'}\, u_j^{'}} \;=\; \overline{u_i^{'}\, u_j^{'}}. \tag{19}$$

It is now possible to extend, in a straightforward manner, the present multifractal model for the subgrid-subgrid stresses, $\overline{u_i^{sgs}\, u_j^{sgs}}$ in the LES equations to the Reynolds stresses of the RANS equations. This derivation makes the single simplifying assumption that all scales between the grid scale $\Delta$ and the viscous scales are inertial-range scales of the turbulent flow field. This assumption will be approximately true in high Reynolds-number turbulence. If so, we can then use a Kolmogorov-type spectral analysis of the enstrophy field to determine the total amount of enstrophy $Q^{'}$ in the fluctuation field as

$$Q^{'} = \int_{\overline{k}}^{k_\nu} \mathcal{Q}(k)\, dk \;=\; \frac{3}{4}\, Q_\Delta \left[ \left( \frac{k_\nu}{\overline{k}} \right)^{\frac{4}{3}} \quad 1 \right]. \tag{20}$$

We can then describe the spatial distribution of vorticity magnitudes within the fluctuation field by way of a multiplicative cascade, like the one used previously in our LES subgrid-scale derivation. Similarly, an additive cascade can be used to represent the isotropic decorrelation of vorticity orientations within the fluctuation field from the orientation of the smallest scale within the mean flow. Then, the representation of the spatial distribution of vorticity magnitudes and orientations may be combined with the Biot-Savart operator to obtain an integral expression for the fluctuation velocity field $\boldsymbol{u}^{'}$. Finally, by discretizing the integral, applying central-limit

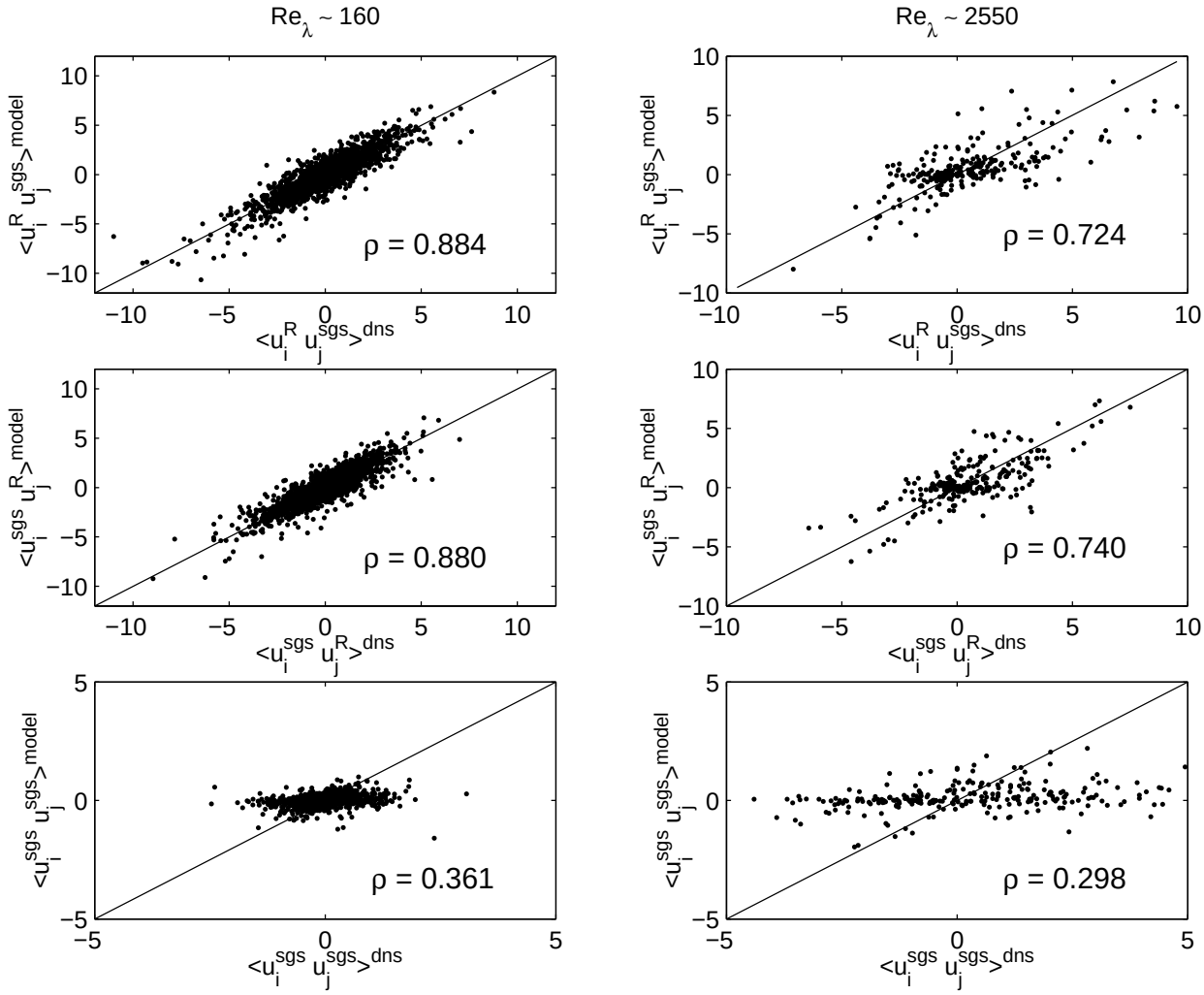


**Fig. 5 Individual terms in the decomposition of $\tau_{ij}^*$ defined in (4), comparing DNS vs. model values in the lower and higher Reynolds-number contexts. Both of the resolved-subgrid terms ($\overline{u_i}\,\overline{u_j^{sgs}}$ and $\overline{u_i^{sgs}}\,\overline{u_j}$, *top* & *middle*) produced correlations of $\rho \sim 0.858$ and $\rho \sim 0.726$, respectively. Mean normalized $L^2$ errors for these terms were calculated to be $0.797$ and $0.963$, respectively. The Subgrid-Subgrid term ($\overline{u_i^{sgs}}\,\overline{u_j^{sgs}}$, *bottom*), however, exhibits lower correlations ($\rho \sim 0.361$ and $\rho \sim 0.298$) and higher $L^2$ errors ($1.460$ and $1.182$) in the low and high-Re cases, respectively. This indicates that the present model may not capture completely subgrid-subgrid interactions. We are presently evaluating certain higher-order refinements to the model to address these issues.**

concepts, and taking the high Reynolds-number limit (*i.e.* the same reasoning by which our multifractal LES model was derived), the fluctuation field $\boldsymbol{u}'$ can be represented as

$$u_i' \sim C_{\mathcal{M}} |\overline{U}| \left[\frac{Q'}{\overline{Q}}\right]^{\frac{1}{2}} \overline{\hat{e}_i}, \qquad (21)$$

where $\overline{\hat{\mathbf{e}}}$ represents the orientation of the velocity field at the smallest scales of the mean flow. As a result, the Reynolds stresses can be expressed using multifractal concepts as

$$\widetilde{u_i' u_j'} \sim \overline{C_{\mathcal{M}}^2 \left(|\overline{U}|\right)^2 \frac{Q'}{\overline{Q}} \overline{\hat{e}_i}\,\overline{\hat{e}_j}}. \qquad (22)$$

The resulting model is a simple algebraic expression, readily determined from the resolved scales of an LES calculation. As such, its implementation would be no more computationally burdensome than presently-existing algebraic RANS models.

The proposed multifractal model for the Reynolds stresses, however, represents a fundamental departure from most traditional RANS models. Prior RANS modeling efforts have relied largely on the gradient-transport hypothesis and associated eddy-viscosity assumptions to relate the Reynolds stresses back to parameters of the mean flow. By contrast, the present multifractal model makes no assumption that the transport of $u_i'$ momentum is related directly to the orientation of the mean-flow gradients and the action of small-scale stochastic eddies within

the turbulent flow field. As such, the model abandons the traditional assumption that the orientation of the Reynolds-stress tensor coincides with that of the mean-strain field. Instead, by taking the orientation of the smallest scale of the mean flow as a departure point for describing an isotropic decorrelation of the Reynolds stresses through the fluctuation field, the multifractal model remains more consistent with the decorrelation process observed in true hydrodynamic turbulence, discussed in our previous paper. The model also abandons the traditional analogy between viscous stresses in Newtonian fluids and Reynolds stresses in turbulent flow, and therefore is able to do away with the eddy-viscosity construct. Instead, the present multifractal model draws on the well-documented multifractal structure of the enstrophy field at inertial-range scales in high Reynolds-number turbulence, and the kinematic relationship between the vorticity and velocity fields embodied in the Biot-Savart law. Thus, the present multifractal model incorporates comparatively more of the dynamics present in real hydrodynamic turbulence than most classical RANS closure models.

**5. Concluding Remarks.**

The foregoing *a priori* analysis of a multifractal model for large-eddy simulation suggests that, in both lower and higher Reynolds-number contexts, the present model recovers significant structural characteristics of the subgrid stress tensor and SGS energy production fields. Correlations for the SGS stress tensor $\tau_{ij}^*$ were calculated to be $\rho \sim 0.855$ and $\rho \sim 0.653$ in the lower and higher Reynolds-number cases, respectively. Correlations between model and DNS values of the subgrid energy-production field $\mathcal{P}^*$ were reported to be $\rho \sim 0.860$ and $\rho \sim 0.804$ for the lower and higher Reynolds-number flows. We also reported high correlations $\rho \sim 0.91$ and low $L^2$ errors for the filtered subgrid-velocity components $\overline{u_i^{sgs}}$, a fundamental test of the present multifractal model, which explicitly represents the subgrid-velocity field. Finally, analyses of the individual terms within the stress-tensor decomposition in (4) suggest that the model captures much of the resolved-subgrid field interactions. Lower correlations and greater $L^2$ errors for the subgrid-subgrid term, however, indicate that the model is less able to recover subgrid-subgrid interactions within the flow. These observations have suggested certain refinements to the model, which we are currently evaluating. Finally, we have also outlined a multifractal model for the Reynolds stresses in the Reynolds averaged Navier-Stokes equations, which extends the multifractal approach for large-eddy simulation to turbulence-closure modeling in the RANS setting.

*Acknowledgments*

*The authors gratefully acknowledge the financial support provided by the François-Xavier Bagnoud Foundation, Sion, Switzerland. The DNS data for this study were generously provided by the Center for Turbulence Research at Stanford University and the NASA Ames Research Center, Moffet Field, California.*

## References

[1]E. Aurell, U. Frisch, J. Lutsko and M. Vergassola. On the multifractal properties of the energy dissipation derived from turbulence data. *J. Fluid Mech.*, 238:467-486, 1992.

[2]J. Bardina, J.H. Ferziger and R.S. Rogallo. Improved subgrid models for large eddy simulation. *AIAA*, Paper 80-1357, 1980.

[3]J.G. Brasseur, and C.H. Wei. Interscale dynamics and local isotropy in high Reynolds number turbulence within triadic interactions. *Phys. Fluids* 6:842-870, 1994.

[4]K.A. Buch and W.J.A. Dahm. Experimental study of the fine-scale structure of conserved scalar mixing in turbulent flows. Part 2. $Sc \sim 1$. *J. Fluid Mech.*, 364:1-29, 1998.

[5]G.C. Burton, W.J.A. Dahm, D.R. Dowling and K.G. Powell. A New Multifractal Subgrid-Scale Model for Large-Eddy Simulation. *AIAA*, Paper 2002-0983, 2002.

[6]A.B. Chhabra, and K.R. Sreenivasan. Scale-invariant multiplier distributions in turbulence. *Phys. Rev. Lett.*, 68:2762-2765, 1992.

[7]J.A. Domaradzki, and E. M. Saiki. A subgrid-scale model based on the estimation of unresolved scales of turbulence. *Phys. Fluids*, 9:2148-2164, 1997.

[8]J.A. Domaradzki, and K. Loh. The subgrid-scale estimation model in the physical space representation. *Phys. Fluids*, 11:2330-2342, 1999.

[9]K. Falconer *Fractal Geometry: Mathematical Foundations and Applications.* John Wiley & Sons, 1990.

[10]M. Farge, K. Schneider, and N. Kevlahan. Non-gaussianity and coherent vortex simulation for two-dimensional turbulence using an adaptive orthogonal wavelet basis. *Phys. Fluids*, 11:2187-2201, 1999.

[11]R.D. Frederiksen, W.J.A. Dahm, and D.R. Dowling. Experimental assessment of fractal scale similarity in turbulent flows. Part 1. One-dimensional intersections. *J. Fluid Mech.*, 327:35-72, 1996.

[12]R.D. Frederiksen, W.J.A. Dahm, and D.R. Dowling. Experimental assessment of fractal scale similarity in turbulent flows. Part 3. Multifractal scaling. *J. Fluid Mech.*, 338:127-155, 1997.

[13]U. Frisch. *Turbulence: The Legacy of A.N. Kolmogorov.* Cambridge University Press, 1995.

[14]M. Germano. A proposal for a redefinition of the turbulent stresses in the filtered Navier-Stokes equations. *Phys. Fluids*, 29:2323-2324, 1986.

[15]M. Germano, U. Piomelli, P. Moin, and W.H. Cabot. A dynamic subgrid-scale eddy viscosity model. *Phys. Fluids*, A3:1760-1765, 1991.

[16]B.J. Geurts Inverse modeling for large-eddy simulation. *Phys. Fluids*, 9:3585-3587, 1997.

[17]J. Jimenez, A.A. Wray, P.G. Saffman, and R.S. Rogallo The Structure of Intense Vorticity in Isotropic Turbulence. *J. Fluid Mech.*, 255:65-90, 1993.

[18]R.M. Kerr, J.A. Domaradzki, and G. Barbier. Small-scale properties of nonlinear interactions and subgrid-scale energy transfer in isotropic turbulence. *Phys. Fluids*, 8:197-208, 1996.

[19]R. Kraichnan. Models of intermittency in hydrodynamic turbulence. *Phys. Rev. Lett.*, 65:575-578, 1990.

[20]S. Liu, C. Meneveau, and J. Katz. On the properties of similarity subgrid-scale models as deduced from measurements in a turbulent jet. *J. Fluid Mech.*, 275:83-119, 1994.

[21]J. Mansfield, O. Knio, and C. Meneveau. A dynamic LES scheme for the vorticity transport equation: formulation and *a priori* tests. *J. Comp. Phys.*, 145:693-730, 1998.

[22]C. Meneveau, and K.R. Sreenivasan. Simple multifractal cascade model for fully developed turbulence. *Phys. Rev. Lett.*, 59:1424-1427 (1987).

[23]C. Meneveau, and K.R. Sreenivasan. The multifractal nature of turbulent energy dissipation. *J. Fluid Mech.*, 224:429-484, 1991.

[24]C. Meneveau. Analysis of turbulence in the orthonormal wavelet representation. *J. Fluid Mech.*, 232:469-520, 1991.

[25]C. Meneveau, T. Lund, and W. Cabot. A Lagrangian dynamic subgrid-scale model of turbulence. *J. Fluid Mech.*, 319:353-385, 1996.

[26]O. Metais, and M. Lesieur. Spectral large-eddy simulation of isotropic and stably stratified turbulence. *J. Fluid Mech.*, 239:157-194, 1992.

[27]A. Misra, and D.I. Pullin. A vortex-based subgrid stress model for large eddy simulation. *Phys. Fluids*, 9:2443-2454, 1997.

[28]H. Peitgen, H. Jurgen, and D. Saupe. *Chaos and Fractals: New Frontiers of Science*. Springer-Verlag (1992)

[29]R.R. Prasad, C. Meneveau, and K.R. Sreenivasan. The multifractal nature of the dissipation field of passive scalars in fully turbulent flows. *Phys. Rev. Lett.*, 61:74-77 (1988)

[30]R.R. Prasad, and K.R. Sreenivasan. Quantitative three-dimensional imaging and the structure of passive scalar fields in fully turbulent flows. *J. Fluid Mech.*, 216:1-34 (1990)

[31]D.I. Pullin, and P.G. Saffman. Reynolds stresses and one-dimensional spectra for a vortex model of homogeneous anisotropic turbulence. *Phys. Fluids*, 6:1787, 1994.

[32]P. Sagaut. *Large-Eddy Simulation for Incompressible Flow*. Springer-Verlag (2000)

[33]A. Scotti, and C. Meneveau. Fractal model for coarse-grained nonlinear partial differential equations. *Phys. Rev. Lett.*, 78:867-870, 1997.

[34]A. Scotti, and C. Meneveau. A fractal model for large eddy simulation of turbulent flow. *Physica D*, 127:198-232, 1999.

[35]J. Smagorinsky. General circulation experiments with the primitive equations: I. The basic equations. *Mon. Weather Rev.*, 91:99-164, 1963.

[36]K.R. Sreenivasan, and R.R. Prasad. New results on the fractal and multifractal structure of the large Schmidt number passive scalars in fully turbulent flows. *Physica D*, 38:322-329 (1989).

[37]K.R. Sreenivasan. Fractals and multifractals in fluid turbulence. *Annu. Rev. Fluid. Mech.*, 23:539-600, 1991.

[38]K.R. Sreenivasan. On local isotropy of passive scalars in turbulent shear flows. *Proc. R. Soc. Lond. A*, 434:165-182, 1991.

[39]K.R. Sreenivasan, and G. Stolovitzky. Turbulent cascades. *J. Stat. Phys.*, 78:311-333, (1995).

[40]S. Stoltz, and N.A. Adams An approximate deconvolution procedure for large-eddy simulation. *Phys. Fluids*, 11:1699-1701, 1999.

[41]Y. Zang, R.L. Street, and J. Koseff. A dynamic mixed subgrid-scale model and its application to turbulent recirculating flows. *Phys. Fluids*, A5:3186-3196, 1993.